journal of the international meteor organization

WGN

51:2
april 2023

Call for future IMCs
Estimating magnitude ratio using video observations
Artificial meteoroid re-entry simulations
"Flying Fish" fireball of 2014 July 17
Remarkable meteors from the PatrICIA project

ISSN 1016-3115

WGN Vol. 51, No. 2, April 2023, pp. 23 – 44

Conferences

Ongoing Meteor Work

Front and back cover photos

Fireball caused by the atmospheric entry of the asteroid 2023 CX_1 on 2023 February 13, 02^h59^m UT, photographed from the south of the Netherlands. Nikon D850 camera was used with 135-mm lens at f/6.3, and 30 s exposure at ISO 400. Photo courtesy: Gijs de Reijke.

More than 20 meteorites were recovered from the fall in the Normandy region of France, with masses ranging from 2 to 350 g.

Writing for WGN

This Journal welcomes papers submitted for publication. All papers are reviewed for scientific content, and edited for English and style. Instructions for authors can be found in WGN **45:1**, 1–5, and at `http://www.imo.net/docs/writingforwgn.pdf` .

Copyright

Legal address

International Meteor Organization, Jozef Mattheessensstraat 60, 2540 Hove, Belgium.

Conferences

Call for future IMCs: 2024 IMC

Cis Verbeeck and Marc Gyssens

The IMO cordially invites candidate IMC organizers to present proposals to organize the International Meteor Conference in 2024. To give interested parties full opportunity to prepare themselves it is important to plan future IMCs well in advance. If you are interested in organizing the IMC 2024 or a later edition, please contact Cis Verbeeck (`cis.verbeeck@gmail.com`) at your earliest convenience. He will provide you with detailed documentation which describes all aspects of an IMC. This documentation does not only describe a scenario for organizing an IMC, but also contains useful documents, templates and detailed statistics on past IMCs answering most questions future IMC organizers may encounter. We are aware that organizing an IMC involves a wide range of organizational and financial responsibilities, and, therefore, the IMO wants to assist future IMC organizers to the best of its abilities. Also these financial aspects are amply covered in the documentation we can provide, with complete examples of past IMC proposals and budgets.

An IMC always takes place from Thursday evening (arrival of the participants) to Sunday lunchtime (departure of the participants). The period of the year in which the IMC is held is typically in September, although this can be stretched from the end of August to early October. Occasionally, we have had IMCs at different times of the year, but this should always have a very good reason (for example, allowing participants to combine their participation with participating in another major meteor-related conference nearby). By the same token, we of course want to avoid that the IMC overlaps with other major conferences in the same field. In 2024, for example, we wish to avoid overlap with the Europlanet Science Congress (EPSC), which takes place in the period September 8–13.

Detailed proposals are due 2023 July 1, and should be sent to `cis.verbeeck@gmail.com`, preferably in PDF-format or a Word document. The following questions should certainly be answered in your application:

- **Who will organize the IMC?** Who is going to be the local organizer? Team work is essential for the local organizing committee and therefore you should indicate who will be part of a Local Organizing Committee. Prior experience with organizing conferences is of course an asset.

- **Why do you want to do it?** What is your motivation to organize an IMC? You may have particular reasons to organize an IMC, such as anniversary of the organizing group, and this may favor the selection of your proposal.

- **Can it be postponed?** We can only have one IMC every year. Sometimes, we receive multiple offers for organizing an IMC in a particular year. Of course, we wish to honor all solid proposals, but this is only possible if you as an organizer are flexible and are also willing to consider organizing your IMC in a subsequent year. If there are reasons why the application cannot be postponed, please describe these reasons clearly! Acceptable reasons can be an important anniversary of your group, the absence of external funding in other years, or restrictions on the availability of the infrastructure you have in mind.

- **Where do you want to do it?** Which location do you have in mind to organize an IMC? Why is this a good location? Can it easily be reached by plane, public transportation, and/or car? How many hours is it by public transportation from the nearest major international airport and/or train station? Can the organizers provide a shuttle service from there to the conference and back?

  Provide a few pictures of the location, or, a web link to such pictures. Preferably, lectures and accommodation should be under the same roof, but there is no real objection to the lecture room being at a separate location within easy walking distance from the accommodation. Describe the accommodation at your disposal. A suitable lecture room is of course essential. It is important that you can darken the lecture room sufficiently so that presentations can be followed comfortably and that details in photographs are not blurred by unwanted incoming daylight. Besides being a place where meteor workers exchange information about their work via lectures and posters, an IMC is also a place where meteor workers *meet* each other. This latter aspect of an IMC is almost as important as the former to improve bonding within the international meteor community. Therefore, there should be a bar or a room that be can organized as such where people can socialize. Many meteor workers meet each other once a year at best, and often only once every so many years. Therefore, it should not come as a surprise that this socializing can often go on until the wee hours of the morning. So, make sure your bar facility does not have to close at 10 p.m., for instance!

Additionally, please provide some information of the availability of alternative accommodation within the vicinity of the IMC location. Some participants prefer to arrange their own accommodation, especially if they want to come with their family.

- **What will it cost?** With respect to the expenditures, take into account that the participants must be offered full board from Thursday evening, dinner, up to Sunday, lunch, inclusive. Of course, lecture room facilities should be accounted for, as well as a coffee break in the morning and in the afternoon. Finally, it is also customary to have a half-day excursion (max. 6 hours), usually on Saturday afternoon. Take into account that the registration fee including full board in a multiple room should not exceed 250 EUR per person by much. This price does not include t-shirts or printed proceedings, which can be ordered separately. Draft a preliminary budget for the IMC proposed. Mention all sources of income, in particular sponsors or subsidies. As future prices for accommodation may not yet be available at the moment of your candidacy, work with current prices corrected for expected inflation and take into account exchange rate fluctuation against Euro if that is applicable.

  Note that, although the IMO provides the service of collecting the registration fees for you, the IMO will in principle *not* cover any negative balance that you might incur, so, please, draft your budget responsibly! A realistic budget is an essential element in the evaluation of your proposal.

We wish to conclude with two important remarks:

- First-hand experience obtained by attending an IMC is very important, because that is the best way to find out how an IMC works and what is really important. If nobody of the organizing group has attended an IMC recently, we strongly encourage you to make sure that several of them participate in a IMC prior to the one you wish to organize!

- If you experience major difficulties with meeting some of the requirements, contact Cis Verbeeck already before the deadline of July 1 for submitting your proposal. In this way, we can give you some valuable feedback which may strengthen your proposal.

We look forward to hear from candidate IMC organizers for 2024 or later conferences! The decision about the 2024 IMC will be taken by the IMO Council no later than 2023 August 30.

IMO bibcode WGN-512-verbeeck-futureimcs NASA-ADS bibcode 2023JIMO...51...23V

Ongoing Meteor Work

An attempt to estimate the magnitude ratio using video observations in the case of eight minor showers listed in the 2023 IMO Meteor Shower Calendar

Masahiro Koseki[1]

Video observations naturally cannot catch all meteors and it is necessary to compensate the raw meteor number by the perception coefficient to get the real magnitude distribution as is done with visual observations. If we suppose the perception coefficient of shower meteors is the same as that for sporadic meteors, we can calculate the relative magnitude ratio of the shower $r_{Relative}$. We can write the relation of the ratio between the numbers of shower and sporadic meteors, N_{Shower} and $N_{Sporadic}$, with the absolute magnitude M_a as $\log(N_{Shower}(M_a)/N_{Sporadic}(M_a)) = a * M_a + \text{constant}$ and $\log r_{Relative} = a$. This $r_{Relative}$ can be the index to the magnitude distribution of meteor showers; smaller $r_{Relative}$ means that the brighter meteors are rich in the stream and larger the reverse. If we can get the magnitude ratio of sporadic meteors, we can get the magnitude ratio easily: $r = r_{Relative} * r_{Sporadic}$.
We applied this method to the eight minor meteor showers listed in the IMO Meteor Shower Calendar 2023 and confirmed the validity of our method.

Received 2022 December 28

1 Introduction

The magnitude ratio, sometimes referred to as the 'population index', is one of the most important indexes to understand the particle distribution in meteoroid streams. Attempts to evaluate the magnitude ratio have been carried out through visual meteor observations, for example, Kresáková (1966). She estimated probabilities for the individual magnitude using the magnitude ratio of sporadic meteors $r = 3.4$ from visual results and many visual observers have used them to calculate the magnitude ratios. But there is no probability function (perception coefficient) for video observations because video devices differ greatly from each other in their observations.

Using SonotaCo net observations, we estimate the magnitude ratios for eight minor streams:
#0404 GUM, #0145 ELY, #0183 PAU, #0206 AUR, #0281 OCT, #0023 EGE, #0022 LMI, and #0246 AMO.

2 Magnitude distribution of sporadic meteors and shower meteors

Figure 1 shows the magnitude distribution of #0145 ELY and of sporadic meteors in the same period; we select shower meteors by ourselves but use sporadic meteors as classified by the SonotaCo network (SonotaCo, 2009; SonotaCo et al., 2021). Both distributions show a bend around absolute magnitude Ma=0, because video observations miss fainter meteors just as visual observers do. The magnitude distribution of #0145 ELY does not seem to be linear even in the brighter range and we cannot calculate the magnitude ratio of #0145 ELY directly. If we presume the perception probability is the same in shower meteors as in sporadic meteors, we could use the ratio between them as the index for the magnitude ratio.

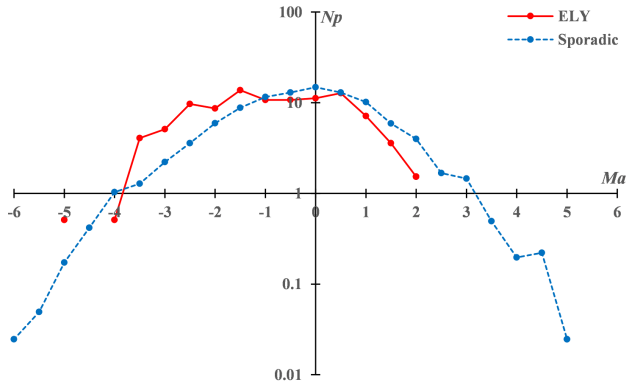

Figure 1 – Magnitude distribution of #0145 ELY and sporadic meteors. The y-axis is scaled as a common logarithm and shows the percentage of the total at each value of *Ma*.

We calculate the ratio of the number of #0145 ELY meteors to the number of sporadic meteors, as a function of the absolute magnitude (Figure 2, left panel #0145 ELY). This ratio seems to be linearly distributed and suggests our presumption on the perception probability is correct. The ratio decreases with the absolute magnitude. This means the fainter meteors in #0145 ELY are fewer and the brighter meteors in #0145 ELY increase in terms of the absolute magnitude, compared with sporadic meteors. The slope a can be an index to the magnitude distribution in meteor showers and we call 10^a the relative magnitude ratio $r_{Relative}$.

If we use the magnitude distribution of sporadic meteors brighter than $Ma < -2.5$ (Figure 2, right panel Sporadic), we can easily calculate the magnitude ratio of sporadic meteors using the slope 0.55835 shown in the figure. Both y-axes in Figure 2 are expressed as common logarithms; therefore, we get $r_{SPO} = 10^{0.55835} = 3.62$. Then we can find the magnitude ratio of #0145 ELY

[1]The Nippon Meteor Society (NMS), 4-3-5 Annaka, Annaka-shi, Gunma-ken, 379-0116 Japan. Email: geh04301@nifty.ne.jp

IMO bibcode WGN-512-koseki-ratio
NASA-ADS bibcode 2023JIMO...51...25K

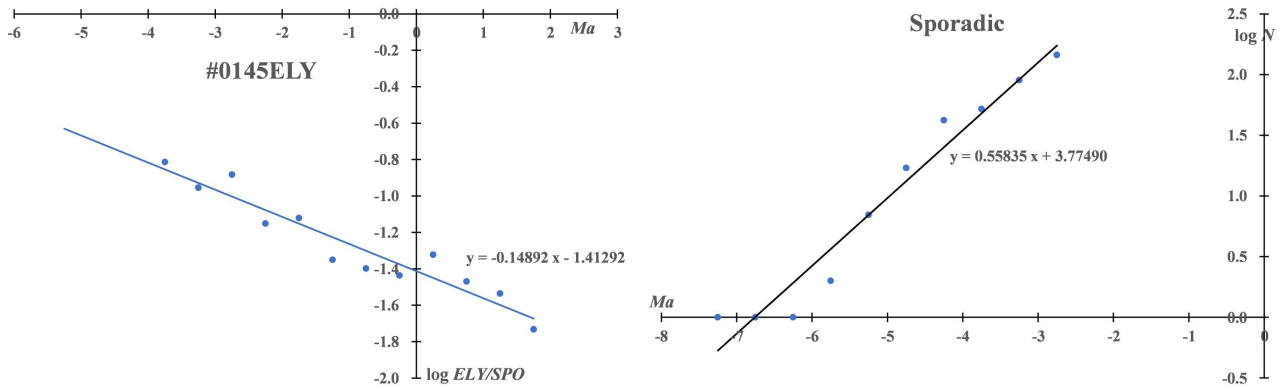

Figure 2 – Relative magnitude distribution of #0145 ELY to sporadic meteors (left: #0145 ELY) and magnitude distribution of sporadic meteors that are a part of Figure 1 (right: Sporadic). Both y-axes are scaled as common logarithms.

Table 1 – Estimated magnitude ratios for the eight minor meteor streams. Period gives the solar longitude of the start and the end of observations used here, N is the number of the shower meteors classified in this study.

Name		GUM	ELY	PAU	AUR	OCT	EGE	LMI	AMO	Mean
r_{IMO}		3.0	3.0	3.2	2.5	2.5	3.0	3.0	2.4	2.83
r_{Video}	r_{SPO}	3.66	3.62	3.73	3.46	3.38	3.78	4.38	3.03	3.63
	$r_{Relative}$	0.94	0.71	1.12	0.73	0.64	0.74	0.62	0.58	0.74
	r_{Shower}	3.46	2.57	4.18	2.53	2.17	2.81	2.71	1.75	2.77
Period	Start	295	45	130	153	192.0	185	204	236.3	
	End	305	55	140	163	193.0	230	214	242.3	
N		73	196	59	118	51	548	323	90	

in the magnitude range between −4 and +2 using the slope of Figure 2 (left panel #0145 ELY). Again because both y-axes in Figure 2 are expressed as common logarithms, we can get $r_{Relative} = 10^{-0.14892} = 0.71$, then r_{Shower}=$r_{Relative}$*r_{SPO}=2.57.

In the same way, we can estimate the magnitude ratio of the other seven minor streams (Table 1).

If we need to know what is the portion of the bright meteors in a meteor shower, it is enough to calculate the relative magnitude ratio $r_{Relative}$. This calculation is very simple, and we can use a wider magnitude range compared to the usual way of determining the population index, as we described above. But if we want to know the magnitude ratio of the meteor shower itself, it would be necessary to know the perception coefficient or the magnitude ratio of sporadic meteors.

We understand the estimation of the magnitude ratio of sporadic meteors is a very important subject to get the magnitude ratio of a meteor stream. But the magnitude ratio of sporadic meteors is not constant with meteor velocity and the different photometric systems used in different groups make the problem confusing. In the next section, we will study a better way to estimate the sporadic magnitude ratio and those of shower meteors.

3 Magnitude ratio of sporadic meteors

It should be emphasized first that the numbers given here are specific to the SonotaCo network, as different observation groups have different definitions of shower meteors and different photometry systems. It would be interesting to compare the magnitude ratios derived from different groups. But we concentrate here on describing how to calculate the magnitude ratio even if we may not present the definitive one. We select three factors that may cause differences in the magnitude ratio of sporadic meteors: seasonal variation and velocity (corresponding to their origin), and year-to-year variation.

3.1 Seasonal variation

We divide the data into four groups: solar longitude λ_s=0–90 (spring), λ_s=90–180 (summer), λ_s=180–270 (autumn), and λ_s=270–360 (winter). Figure 3 shows the magnitude distributions of these four groups as percentages of the total number, on a logarithmic scale.

The differences become larger in the ranges brighter than magnitude −6 and fainter than magnitude +3 because the data are sparse in both ranges. The peaks of

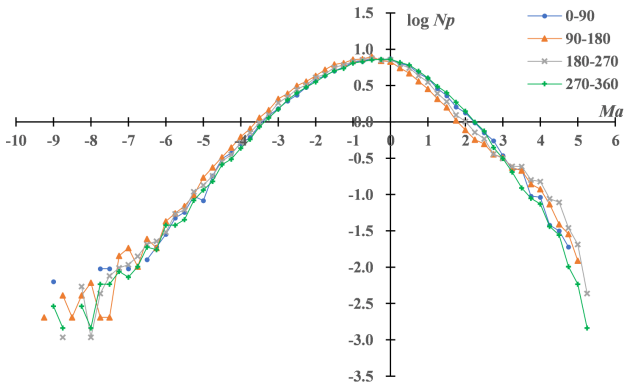

Figure 3 – Variation of the magnitude distributions in the four seasons: λ_s=0–90 (spring), λ_s=90–180 (summer), λ_s=180–270 (autumn), and λ_s=270–360 (winter).

Table 2 – Seasonal variation of the magnitude ratio of sporadic meteors.

λ_s	0–90	90–180	180–270	270–360
r_{SPO}	3.59	3.63	3.56	3.63

the magnitude distributions of winter and spring are a little bit (about −0.5 magnitude) brighter than summer and autumn. But the slopes of the distribution are almost the same, that is, about 0.56. It is suggested that we can regard the magnitude ratio of sporadic meteors as constant year-round (Table 2).

3.2 Year-to-year variation

We calculate the magnitude ratios for two magnitude ranges, $-6 < Ma < -2$ (A) and $-5 < Ma < -3$ (B) (see Table 3), to check the data consistency. Fainter meteors around $Ma = -2$ might be missed and the numbers of meteors brighter than $Ma < -6$ are too small to get a reliable magnitude ratio. The magnitude ratios by A are a little bit smaller than ratios B; a fraction of $Ma = -2$ to -3 meteors might be missed. In the case of B, the magnitude ratios become higher, but the standard deviation becomes larger than in case A because the range is narrower than in case A.

We should note that SonotaCo net observers each use different devices and some of them could be changed at any time. Some prefer a wide view and intend to catch fireballs and some others aim to get accurate orbits by using a long-focus lens. Figure 4 shows an example; the latter observers become active after 2020 and fainter meteors are recorded more. Figure 5 indicates the magnitude ratio decreases with time, but it might be supposed the former observers become active. Though the latter observers do not affect the magnitude ratio so greatly because their impact is in the range $Ma > 0$, the former observers can catch meteors in the wider sky and get bright meteors more than usual. It is necessary to pay close attention to trends caused by the changes in observers' devices over time.

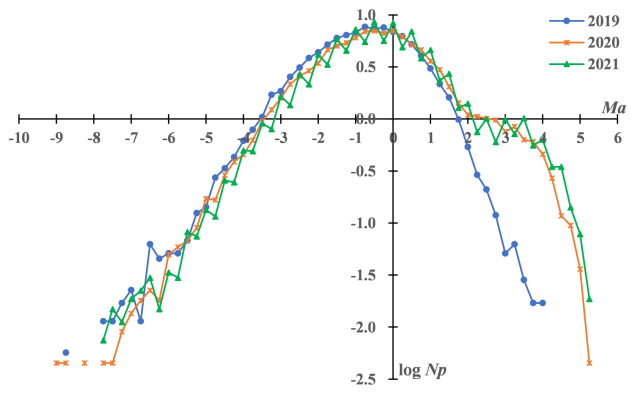

Figure 4 – Comparison of the magnitude distribution in 2019 to 2021.

It is clear from Figure 5 that the observation system has changed, but as can be seen in Table 3, there is no effect on the magnitude range used, and it is considered that there is no change over time in the magnitude ratio. The probable range of the magnitude ratio of sporadic

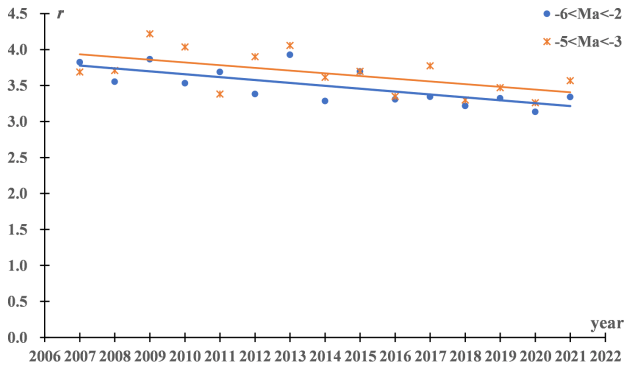

Figure 5 – Change of magnitude ratio in 2007–2021 comparing the difference in the magnitude range used.

meteors might be described as their mean: between $r = 3.50$ (for $-6 < Ma < -2$) and $r = 3.67$ (for $-5 < Ma < -3$).

3.3 Difference due to origin

We know meteor observations indicate two peaks in the geocentric velocity distribution of meteors (Figure 6) and they correspond to their origin; a higher group arises from the apex source and a lower group from the ANT source. Observational techniques are particular to the sources: video observations preferentially detect the apex source, radar observations the Toroidal, and photographs ANT (Koseki, 2015). Though SonotaCo net data emphasize extremely the high-velocity group (Figure 6), we can divide the distribution into two groups easily with a boundary $V_g = 50$ km/s. Slower meteors towards the left in the figure are ANT and Toroidal meteors and faster ones towards the right in the figure are apex sources. When we calculate the magnitude distribution for all sporadic meteors, the results may be different because of the meteor selection in velocity. It is necessary to note that video observations themselves are different from each other in the meteor selection. Though CAMS is more favorable to slower meteors than SonotaCo net (Koseki, 2018), this research relates to SonotaCo net data only.

It is clear the magnitude ratios for these two groups are significantly different; we can calculate $r = 3.22$

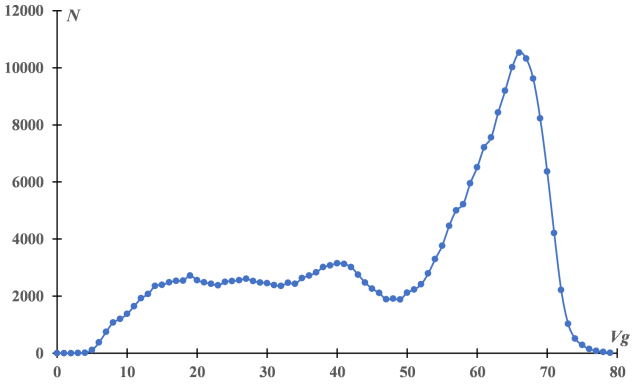

Figure 6 – Velocity distribution of sporadic meteors in SonotaCo net observations. Meteors seem to be divided into two groups at the boundary $V_g = 50$ (km/s).

Table 3 – Change of magnitude ratio in 2007–2021. '$-6 < Ma < -2$' and '$-5 < Ma < -3$' indicate the range used to calculate the magnitude ratio.

Year		2007	2008	2009	2010	2011	2012	2013	2014	2015	2016	2017	2018	2019	2020	2021
$-6 < Ma < -2$	r	3.83	3.55	3.87	3.53	3.69	3.38	3.93	3.29	3.70	3.31	3.34	3.22	3.32	3.14	3.34
$-5 < Ma < -3$	r	3.69	3.71	4.22	4.04	3.38	3.90	4.06	3.61	3.70	3.35	3.78	3.30	3.47	3.26	3.57

Table 4 – Comparison of calculated magnitude ratios based on the different magnitude ratios of the sporadic background.

Name		GUM	ELY	PAU	AUR	OCT	EGE	LMI	AMO	Mean
V_g		29.0	43.7	43.2	65.4	45.6	68.2	61.4	61.7	52.3
r	All	3.69	2.77	4.39	2.85	2.51	2.91	2.42	2.26	2.97
	$V_g < 50$	3.04	2.29	3.62	2.36	2.07	2.40	1.99	1.87	2.45
	$V_g > 50$	4.02	3.02	4.78	3.11	2.74	3.17	2.63	2.46	3.24

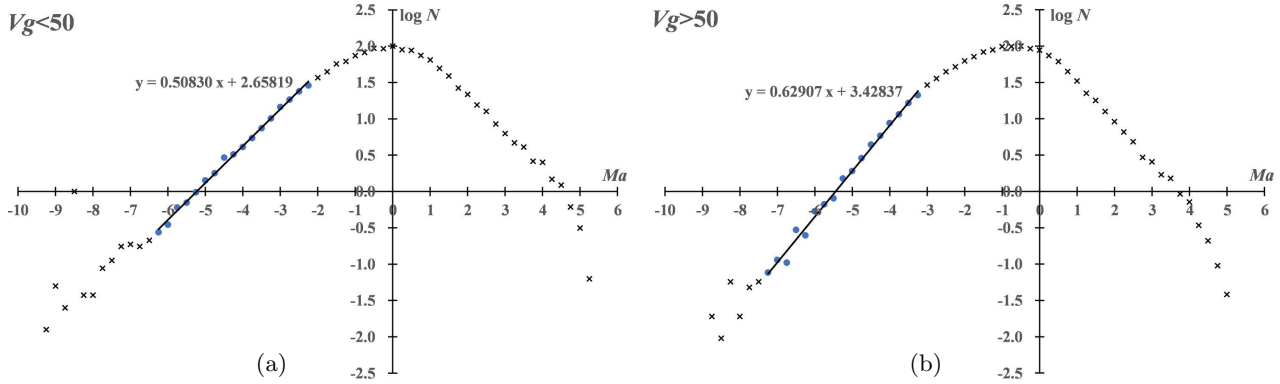

Figure 7 – Magnitude distributions of sporadic meteors. Filled circles are used to calculate the magnitude ratio. Left: $V_g < 50$ km/s (a). Right: $V_g > 50$ km/s (b).

and $r = 4.26$ for the groups $V_g < 50$ km/s and $V_g > 50$ km/s respectively using each slope (Figure 7a and Figure 7b). Though these ratios are from SonotaCo net video observations and may not be reasonable for every observational technique, the magnitude ratios suggest a difference in mass distribution between the origins: the apex source and the ANT source.

Table 4 compares calculated magnitude ratios based on the different magnitude ratios of sporadic meteors; the line 'All' gives the magnitude ratio from the mean magnitude ratio of all sporadic meteors ($r = 3.91$), the lines '$V_g < 50$' and '$V_g > 50$' are for $r = 3.22$ and $r = 4.26$ respectively as mentioned above.

It is suggested the lines $V_g < 50$ and $V_g > 50$ in Table 4 are the limits of the estimated values. The real sporadic magnitude ratio lies between $r = 3.22$ and $r = 4.26$; these are the extreme values; if we use other observational techniques, the mean sporadic magnitude ratio might fluctuate between them.

4 Magnitude ratio and the difference between the mean magnitudes of shower meteors and sporadic meteors

We know three indexes for evaluating the magnitude distribution of meteor showers: magnitude ratio r, relative magnitude ratio $r_{Relative}$, and the difference between the magnitudes of shower meteors and sporadic meteors ΔMa. We try to infer the relation between them using the magnitude ratios for eight minor showers (Table 1) and ΔMa (Table 6): these data are shown in Figure 8a where the best fitting line is also calculated.

Table 5 – The mean magnitude of meteors from seven showers M and corresponding sporadic meteors M_{SPO}, with their magnitude ratios, from Kresáková (1966).

Shower	M	M_{SPO}	r	r_{SPO}	ΔM
LYR	2.97	3.30	2.9	3.5	−0.33
ETA	2.47	3.18	2.3	3.3	−0.71
SDA	2.87	3.16	2.7	3.2	−0.29
PER	2.58	3.25	2.4	3.4	−0.67
ORI	2.95	3.23	2.9	3.4	−0.28
LEO	2.63	3.20	2.5	3.3	−0.57
GEM	2.77	3.23	2.6	3.4	−0.46

Kresáková (1966) gave the difference between the magnitude of shower meteors and sporadic meteors ΔM by visual observations. Table 5 shows a summary of her Table 24 and Figure 8b represents the relation between ΔM and the magnitude ratio r.

We have two clues (from the linear fits in Figure 8a and Figure 8b respectively) to estimate the magnitude ratio of a meteor shower from the mean magnitude and compare the calculated results in Table 6. Though it might be questioned that the relation deduced from visual observations could not be applied to video data directly, the two lines of results in Table 6 are in good

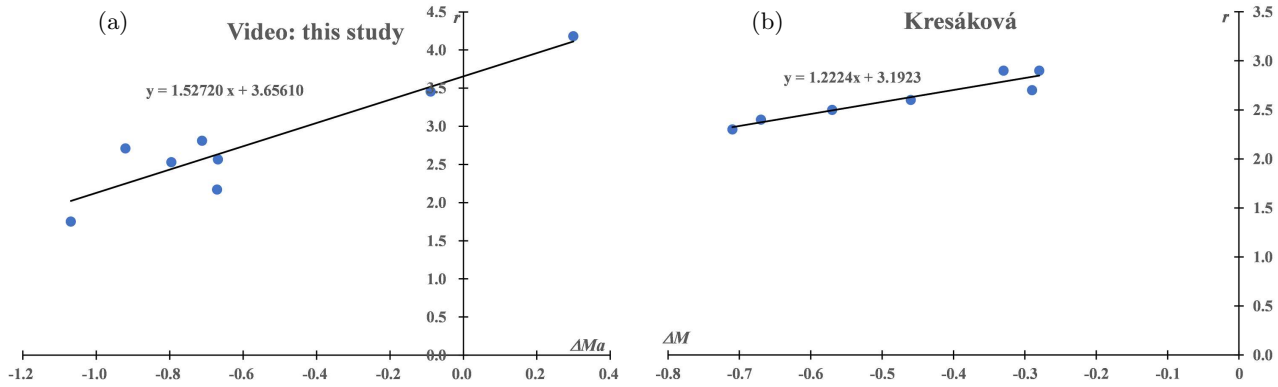

Figure 8 – Magnitude ratio r and the difference between the magnitudes of shower meteors and sporadic meteors ΔMa or ΔM. Left: eight showers in this study (a). Right: seven showers in Kresáková (1966) (b).

Table 6 – Magnitude ratio from the difference between the magnitudes of shower meteors and sporadic meteors. Magnitude ratios r are calculated from video data (Figure 8a) and from visual data (Figure 8b).

Name		GUM	ELY	PAU	AUR	OCT	EGE	LMI	AMO	Mean
Ma	Shower	−0.54	−1.17	−0.52	−1.67	−1.34	−1.39	−1.69	−1.69	−1.25
	Sporadic	−0.46	−0.51	−0.82	−0.88	−0.67	−0.68	−0.77	−0.62	−0.67
	ΔMa	−0.09	−0.67	0.30	−0.80	−0.67	−0.71	−0.92	−1.07	−0.58
r	Figure 8a	3.52	2.63	4.11	2.44	2.63	2.57	2.25	2.02	2.77
	Figure 8b	3.08	2.37	3.56	2.22	2.37	2.32	2.07	1.88	2.49

agreement and we can answer this question that we can indeed apply this method of calculation successfully.

5 Discussion

We assume the perception coefficient is the same both for sporadic meteors and for shower meteors. But the perception coefficient might be different for different meteor velocities as Figure 6 suggests and, therefore, it might be different between shower meteors and sporadic meteors. Though this can be true, this effect seems to be small enough to allow us to neglect it and to estimate the magnitude ratio of a meteor shower. We estimate the perception coefficient PC for SonotaCo net video observations on the assumptions that $r = 3.91$ and PC is 100% for meteors brighter than magnitude −4 using the magnitude distribution of all sporadic meteors (Figure 9). Table 7 gives the summary of the smoothed values of PC. We can then calculate the magnitude ratios for the eight minor streams using this PC (the line 'Perception' in Table 8).

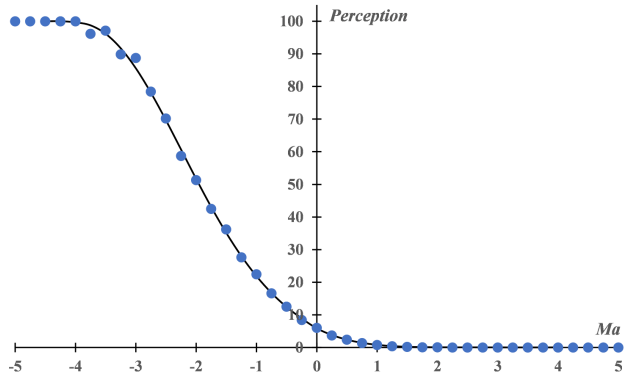

Figure 9 – Estimated perception coefficient of SonotaCo net video observations.

We have estimated the magnitude ratio using the different conditions and can compare them now. The 7 estimations in Table 8 show that the standard deviation naturally becomes larger when the number of meteors N is small. It is suggested that when the number of meteors large enough, $N > 100$, we can get a plausible magnitude ratio using video observations. The IMO Shower Calendar lists the population index, that is, the magnitude ratio, and they basically coincide with our results (Table 8); we listed $S_{CORRESPONDING}$ as r_{Shower} in Table 1.

In conclusion, it is recommended for any video researcher to calculate $S_{CORRESPONDING}$, that is, the magnitude ratio without any assumption of the perception coefficient using the relative magnitude ratio $r_{Relative}$ (see Figure 2 for an example). ΔM_{VISUAL} is an easy way to estimate the magnitude ratio, but this is based on the assumption that video perceptions equal visual ones. The other 5 methods are unique for SonotaCo net video observations and, therefore, could not be applied using values estimated in this study.

References

Brown P., Weryk R. J., Wong D. K., and Jones J. (2008). "A meteoroid stream survey using the Canadian Meteor Orbit Radar. I. Methodology and radiant catalogue". *Icarus*, **195**, 317–339.

Brown P., Wong D. K., Weryk R. J., and Wiegert P. (2010). "A meteoroid stream survey using the Canadian Meteor Orbit Radar. II. Identification of minor showers using a 3D wavelet transform". *Icarus*, **207**, 66–81.

Table 7 – Perception coefficient for SonotaCo net sporadic meteors on the assumptions that $r = 3.91$ and the perception of meteors brighter than magnitude −4 is 100%. *Ma* is absolute magnitude, *PC* is perception coefficient.

Ma	−4.0	−3.5	−3.0	−2.5	−2.0	−1.5	−1.0	−0.5	0.0	0.5	1.0	1.5	2.0	2.5
PC	99.7	96.1	85.6	69.6	51.7	35.1	21.9	12.4	5.9	2.4	0.8	0.2	0.1	0.03

Table 8 – Summary of the estimated magnitude ratios in this study. $S_{CORRESPONDING}$: based on the sporadic meteors during the corresponding period. S_{ALL}: based on all sporadic meteors. $S_{V_g<50}$: based on meteors slower than $V_g < 50$ km/s. $S_{V_g>50}$: based on meteors faster than $V_g > 50$ km/s. ΔM_{VIDEO}: calculated from the magnitude difference between shower meteors and sporadic meteors using the relation in video meteors. ΔM_{VISUAL}: calculated from the magnitude difference using Kresáková's visual data. SD is the standard deviation of the 7 estimations of this study.

Name		GUM	ELY	PAU	AUR	OCT	EGE	LMI	AMO	Mean
N		73	196	59	118	51	548	323	90	
r	IMO	3.0	3.0	3.2	2.5	2.5	3.0	3.0	2.4	2.8
	$S_{CORRESPONDING}$	3.46	2.57	4.18	2.53	2.17	2.81	2.71	1.75	2.77
	S_{ALL}	3.69	2.77	4.39	2.85	2.51	2.91	2.42	2.26	2.97
	$S_{V_g<50}$	3.04	2.29	3.62	2.36	2.07	2.40	1.99	1.87	2.45
	$S_{V_g>50}$	4.02	3.02	4.78	3.11	2.74	3.17	2.63	2.46	3.24
	ΔM_{VIDEO}	3.52	2.63	4.11	2.44	2.63	2.57	2.25	2.02	2.77
	ΔM_{VISUAL}	3.08	2.37	3.56	2.22	2.37	2.32	2.07	1.88	2.49
	Perception	4.32	3.01	3.98	2.72	3.95	2.75	2.54	2.52	3.22
	Mean	3.59	2.67	4.09	2.60	2.63	2.70	2.37	2.11	2.85
	SD	0.43	0.27	0.39	0.29	0.58	0.27	0.26	0.28	0.30

Koseki M. (2015). "What do we see as ANT, Apex and Toroidal sources? — What meteors are, where meteors came from, where meteoroids are going". *WGN, Journal of the IMO*, **43:5**, 127–146.

Koseki M. (2018). "Different definitions make a meteor shower distorted. The views from SonotaCo net and CAMS". *WGN, Journal of the IMO*, **46:4**, 119–135.

Koseki M., Shigeno Y., and Shigeno T. (2022). "A short note on Piscis Austrinids (#0183PAU)". *WGN, Journal of the IMO*, **50:5**, 136–139.

Kresáková M. (1966). "The magnitude distribution of meteors in meteor streams". *Contrib. Astron. Obs. Skalnaté Pleso*, **3**, 75–109.

McCrosky R. E. and Posen A. (1961). "Orbital elements of photographic meteors". *Smithson. Contrib. Astrophys.*, **4**, 15–84.

SonotaCo (2009). "A meteor shower catalog based on video observations in 2007–2008". *WGN, Journal of the IMO*, **37:2**, 55–62. See also "SonotaCo Network Simultaneously Observed Meteor Data Sets", `http://sonotaco.jp/doc/SNM/`.

SonotaCo, Uehara S., Sekiguchi T., Fujiwara Y., Maeda K., and Ueda M. (2021). "J14: A meteor shower and cluster catalog". *WGN, Journal of the IMO*, **49:4**, 76–97.

Whipple F. L. (1954). "Photographic meteor orbits and their distribution in space". *Astron. J.*, **59**, 201–217.

Handling Editor: David Asher

Appendix: Summary notes on the eight minor meteor showers

We analyze the eight minor streams using video observations to confirm the membership of the stream and to obtain the magnitude ratio of the stream. Table A.1 is the by-product of this research, and we hope it might be helpful for readers.

#0404 GUM

#0404 GUM were detected by CMOR2 (Brown et al., 2010) but a meteor photographed by Harvard small cameras in 1950 might be classified as GUM (Whipple, 1954). The activity profile (Figure A.1) suggests about 10 times higher than a usual visual hourly rate. It is natural that only large scale radar and video data can note this activity. Though there are three more active streams in CMOR observations (Brown et al., 2008) southeast of #0404 GUM, that is, #0321 TCB, #0322 LBO, and #0323 XCB, video observations have not noticed them clearly. They might be rich in faint meteors while there might be bright meteors in #0404 GUM though not numerous.

#0145 ELY

#0145 ELY was noticed after C/1983 H1 (IRAS-Araki-Alcock) was discovered but photographic data show this shower was already active in the 1950s (McCrosky & Posen, 1961). The reason why there are no certain visual observations of #0145 ELY before the discovery of the comet is the magnitude ratio and the magnitude distribution of #0145 ELY. They seem to suit photographic and video observations.

Table A.1 – Summary data for the eight meteor streams. λ_s is the longitude of the sun at the maximum, α and δ denote the coordinates of the radiant at the maximum, $\Delta\alpha$ and $\Delta\delta$ are the daily motion of the radiant, V_g is the geocentric velocity at the maximum, e, q, i, ω, Ω are the orbital elements at the maximum.

Name	λ_s	α	$\Delta\alpha$	δ	$\Delta\delta$	V_g	e	q	i	ω	Ω
#0404 GUM	299	228.1	1.30	68.3	−0.82	28.7	0.637	0.950	47.0	204.2	299.0
#0145 ELY	49	290.8	0.09	43.3	0.31	44.1	0.945	1.001	74.9	190.9	49.0
#0183 PAU	135	353.1	0.65	−20.6	0.17	43.2	0.967	0.127	54.9	141.3	315.0
#0206 AUR	158.47	90.7	1.09	39.2	0.12	65.6	0.963	0.678	148.4	109.2	158.5
#0281 OCT	192.57	168.0	—	78.6	—	45.6	0.935	0.991	77.6	168.9	192.6
#0023 EGE	208	103.4	0.86	27.8	−0.13	68.1	0.892	0.757	170.7	240.5	208.0
#0022 LMI	208	158.8	1.07	37.2	−0.29	61.4	0.961	0.619	124.9	103.2	208.0
#0246 AMO	239.8	117.4	0.80	0.8	0.00	61.7	0.963	0.468	133.3	94.2	59.8

#0183 PAU

#0183 PAU is not the traditional 'Piscis Austrinids' reported by visual observers around $\lambda_s = 125$ (Koseki et al., 2022). This activity is very low and could not be recognizable by visual observers. The magnitude ratio suggests this activity suits radar and II (image-intensifier) observations.

#0206 AUR

We know several outbursts were recorded. But we can record a few #0206 AUR meteors around its short maximum in usual years. The magnitude ratio and the short maximum suggest a visual observer can recognize a few bright shower meteors only in the maximum night. The activity of #0206 AUR before $\lambda_s < 157$ and after $\lambda_s > 160$ is uncertain.

#0281 OCT

#0281 OCT is observable in usual years but special in the short activity period. Japanese observers can meet its maximum, but not every year. The activity profile (Figure A.1) is drawn showing the total number of meteors in 15 years (2007–2021) in every $0\overset{\circ}{.}1$ bin. The percentage of shower meteors in all observed meteors is several percent and the magnitude ratio suggests this activity suits video observations. #0281 OCT seems very difficult for visual observers even at its maximum.

#0023 EGE

Although #0023 EGE is a well-known minor meteor shower, it is difficult to recognize its activity clearly because Orionids are near and sporadic meteor activity is high. What is worse, its maximum seems to vary from year to year. The maxima in the activity profile (Figure A.1) are the result of activity in different years. The mean absolute magnitude suggests meteors of #0023 EGE are brighter than Orionids.

#0022 LMI

#0022 LMI has been known as a photographic meteor shower. The magnitude ratio supports this being suited for video and photographic observations. A visual observer can notice its activity at the maximum night because the sporadic activity is sparse around #0022 LMI.

#0246 AMO

We know several outbursts of #0246 AMO but can observe it in usual years. The magnitude ratio suggests the activity of #0246 AMO in usual years suits video observations though a video camera can record one or two shower meteors through one whole night. There are many sporadic meteor activities around #0246 AMO, and #0016 HYD and #0529 EHY confuse observers after $\lambda_s = 242$; the activity profile is not drawn after $\lambda_s > 242$ (Figure A.1).

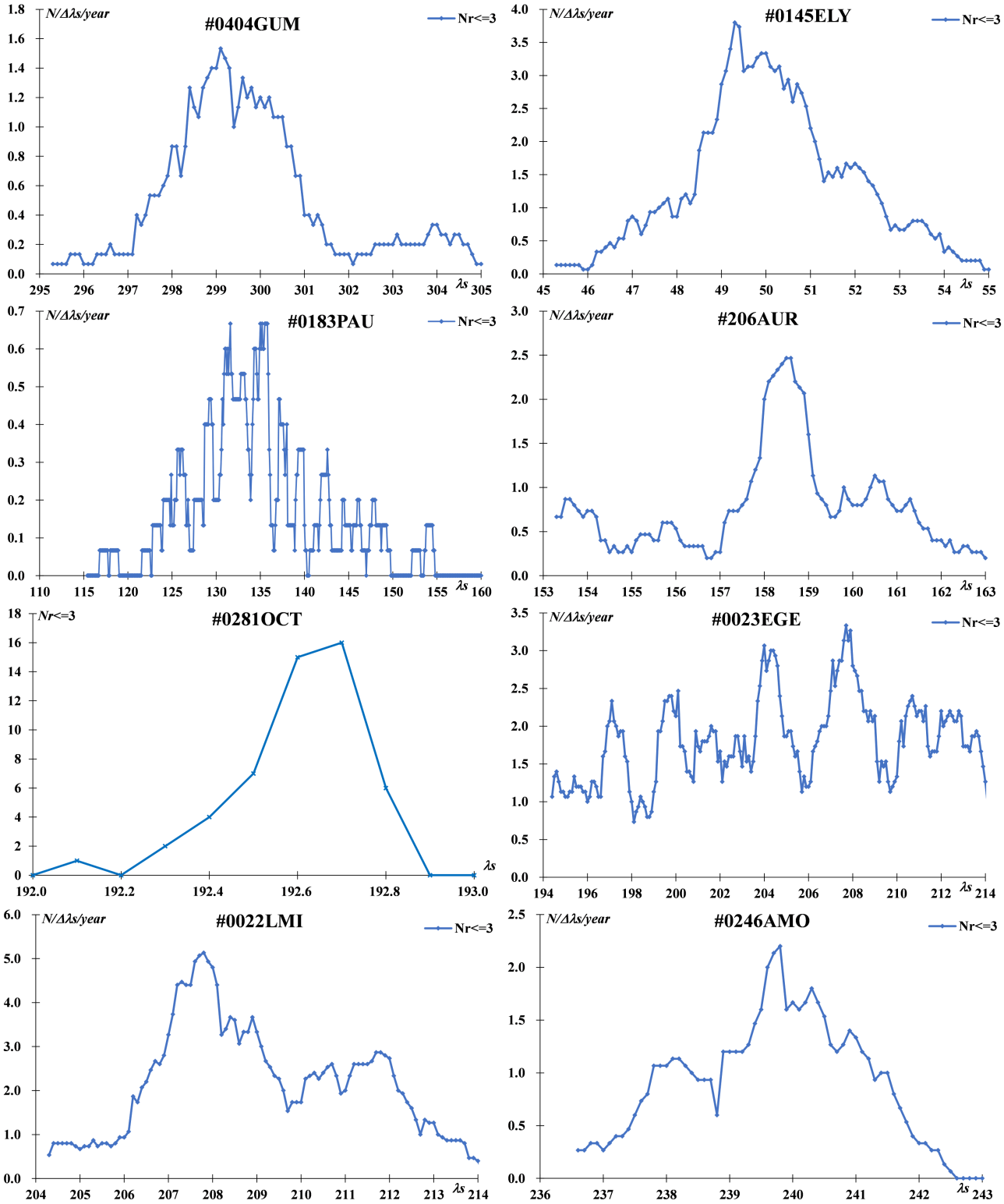

Figure A.1 – The activity profiles of the eight meteor streams calculated by the meteors within 3° from the estimated radiant. The y-axis shows the mean number of shower meteors observed in a day except for #0281 OCT and might suggest about ten times higher value of visual hourly rate.

Artificial meteoroid re-entry simulations for the AllBert EinStein mission

Maximilian Vovk[1], *Detlef Koschny*[1,2], *Michael Frühauf*[1], *Christian Gscheidle*[1], *Valentin Heumann*[1]

The AllBert EinStein mission is intended to re-enter spheres of known size and material into the atmosphere to determine the percentage of kinetic energy converted to light. This paper models the re-entry of multiple artificial meteoroids based on software developed by the ESA's space debris community. An emphasis is placed on determining the best detaching altitude and observer position. Our study shows that the fireballs will be clearly distinguishable depending on the size and properties of the material.

Received 2023 January 24

A Introduction

Most people have probably thought about what would happen if an asteroid were to hit the Earth. If the question has not arisen spontaneously, it might have been prompted by anything from a Hollywood movie to seeing a meteor streak across the sky. Of course, the impact of such an object on our lives will vary significantly depending on size, angle, and other factors. To the extent we want to move beyond starry-eyed speculation towards analysis or even preparation, we need to better understand how these objects interact with our atmosphere.

One way to gather more data would be by simulating these events based on a controlled experiment using an artificial meteor which shape and material characteristics are well-defined (Ceplecha et al., 1998).

In 2022, Michael Frühauf, Christian Gscheidle, and Detlef Koschny have proposed the AllBert EinStein mission. This mission will use multiple decimeter-sized artificial meteoroids of different materials re-entering at about 8 km/s. The AllBert EinStein mission payload will be on a ride-share, and it will be detached from the final stage of the rocket in the re-entry maneuver in order to burn up in the atmosphere (Frühauf et al., 2022). The ball-shaped meteoroids will be kept in place in the fairing by a cage structure designed by Valentin Heumann. Its demise in the re-entry will occur before the fireball of the artificial meteoroid.

In order to run this mission successfully, we had to define the detaching altitude and the observer position of the airborne campaign from which the fireball must be observed. Therefore, we have calculated the light curve of different materials using ESA's re-entry simulation software. The re-entry trajectory has been defined based on ESA's Debris Risk Assessment and Mitigation Analysis (DRAMA) software, while the ablation has been defined based on SpaceCraft Atmospheric Re-entry and Aerothermal Break-up (SCARAB) results.

[1]LRT/TU Munich, Boltzmannstraße 15, 85748 Garching bei München, Germany.
Email: maximilian.vovk@tum.de, d.koschny@tum.de, m.fruehauf@tum.de, c.gscheidle@tum.de, valentin.heumann@tum.de

[2]ESA Near-Earth Objects Coordination Centre, Largo Galileo Galilei 1, 00044 Frascati, Italy.
Email: detlef.koschny@esa.int

IMO bibcode WGN-512-vovk-reentry
NASA-ADS bibcode 2023JIMO...51...33V

B Model definition

For all the simulations, we have considered a set of spherical artificial meteoroids of 5, 10, and 20 cm in diameter re-entering from a Low-Earth Orbit (LEO). We have used initial conditions based on data from the Spectrum rocket by Isar Aerospace to run these simulations. Isar Aerospace has kindly provided the velocity and zenith angle data for each altitude after the de-orbiting burn. The sampler simulation assumes that the Spectrum rocket will de-orbit from a Sun-Synchronous Orbit (SSO) at 500 km.

We have run a set of simulations for different materials, as shown in Table 1. The materials' coefficients considered are required to run the simulations with DRAMA and SCARAB. Except for iron that, as other metallic materials, was already in the European Space maTerIal deMisability dATabasE (ESTIMATE), the rest of the materials' coefficients were defined based on literature data (Abdulagaov et al., 2019; Bouhifd et al., 2007; Gilmour et al., 2020; Hartlieb et al., 2016; Lesher & Spera, 2015; Loehle et al., 2017; Opeil et al., 2020; Szurgot, 2011, 2012). Similar names (e.g., acidic basalt and basic basalt, and carbonaceous and ordinary chondrite) have been given only to differentiate materials with high variability in their coefficients found in literature.

C ESA software

The software developed by ESA's space debris community is called DRAMA, and provides the user with a vast array of tools from space safety to de-orbiting time assessment. One of these tools is SARA, developed by Hyperschall Technologie Göttingen (HTG) on behalf of ESA (Lips et al., 2019). SARA uses an object-oriented approach which speeds up the computations substantially. In this approach, only elementary shapes (i.e., spheres, cylinders, plates, and boxes) are used, where the parent object completely shields the internal components it contains from the incoming heat flux until it has completely dissipated in the re-entry (Kanzler et al., 2017).

However, this software has its limitations. All components have predefined tumble or fixed attitude, and melt while maintaining their shape type in order to make the computations less heavy and to reduce the computation time (Kanzler et al., 2017). The main problem for our mission lies on the ablation mechanism

Table 1 – Set of material properties used for the simulation campaign, where ρ is the material density, T_{melt} the melting temperature, H_{melt} the specific heat of melting, c_p the specific heat capacity, k the heat conductivity, and ε the emissivity coefficient.

Material	ρ $\left[\frac{\text{kg}}{\text{m}^3}\right]$	T_{melt} [K]	H_{melt} $\left[\frac{\text{J}}{\text{kg}}\right]$	c_p $\left[\frac{\text{J}}{\text{kg.K}}\right]$	k $\left[\frac{\text{W}}{\text{m.K}}\right]$	ε [–]
Iron	7870	1808	272 000	440	76.2	0.75
Basalt (acidic)	2400	1257	400 000	1000	1.5	0.83
Basalt (basic)	3100	1533	506 000	1000	1.5	0.83
Ordinary chondrite	3500	1430	265 000	684	3.0	0.83
Carbonaceous chondrite	2800	2000	265 000	1320	1.0	0.83
Granite	2750	1500	250 000	1150	1.2	0.96
Sandstone	2000	1773	680 000	1100	1.5	0.59

used. The temperature T keeps rising based on the specific heat of melting H_{melt}, the heat rate Q, and the specific heat capacity c_p, as shown in Equation (1):

$$\begin{cases} \dfrac{\mathrm{d}m}{\mathrm{d}t} = 0; & \dfrac{\mathrm{d}T}{\mathrm{d}t} = \dfrac{Q}{c_p m}, \quad \text{for } T < T_{\text{melt}}; \\ \dfrac{\mathrm{d}m}{\mathrm{d}t} = -\dfrac{Q}{H}; & \dfrac{\mathrm{d}T}{\mathrm{d}t} = 0, \quad \text{for } T \geq T_{\text{melt}}, \end{cases} \tag{1}$$

where $\mathrm{d}m/\mathrm{d}t$ is the mass loss per time unit.

SARA ablation only starts when the average temperature of the whole body reaches the melting temperature T_{melt}. This does not have important consequences for thin wall structures, but has major effects especially to estimate the mass loss amount solid geometries like our spheres. The heat conductivity coefficient k in the software is used only for the transmission of heat from one base geometry to the other, but not from the parent geometry to the interior child geometries inside. The mass loss, due to the very thick size of the wall structure of solid bodies, often tends to be zero for some materials, since the temperature does not reach in time the melting temperature in the whole body (Lips et al., 2019). For this reason, the SARA computations are very good to determine re-entry trajectory, but are not good enough to determine the ablation mass loss of solid object like meteoroids.

Hyperschall Technologie Göttingen (HTG) also maintains and operates ESA's SCARAB software, which is an expert tool for specific re-entry analysis. SCARAB analyses are offered to European industry and academia as a commercial service by HTG. SCARAB allows modeling complex geometries via a discrete volume panel approach which is more computationally heavy than SARA. For all nodes, temperature, pressure, and heat rate are computed. Each panel will start to melt when it reaches the melting temperature (Lips et al., 2007). To simulate the structure of the artificial meteoroids, we used ten concentric hollow spheres with gradually decreasing diameter. This value has been chosen to reduce the number of panels, and thus the computation time. These ten layers are each 5 mm thick, and are connected to each other so that they can transfer their heat via conduction, as shown in Figure 1.

The inner panel will be influenced by the air convection only when the panel on top has dissipated. SCARAB panel-based calculations are more likely to give realistic results in our approach because the thin-wall

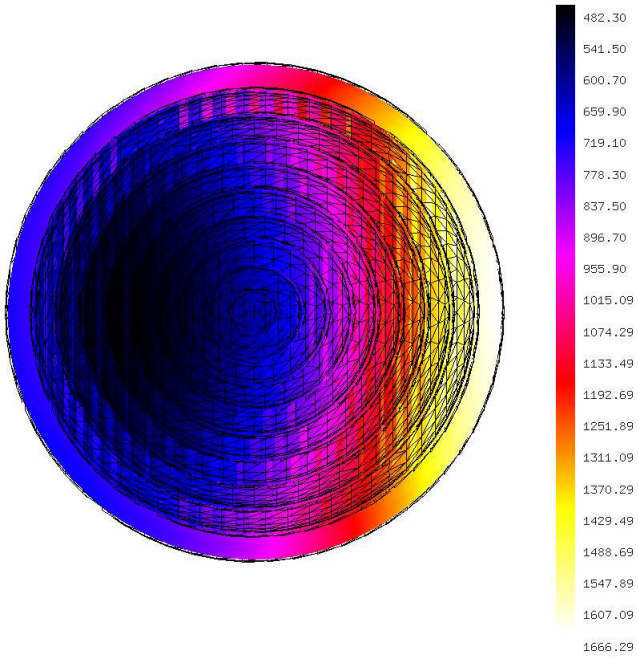

Figure 1 – Temperature distribution (K) inside a ball in a SCARAB simulation. This result shows that the software can simulate a realistic temperature distribution inside a solid object.

assumption on which the software is based is still satisfied. SCARAB re-entry trajectory and ablation results are valid within space debris re-entry velocities of 7–9 km/s; for higher velocities, the ablation results are no longer reliable. For this reason, SCARAB ablation results are not valid for fast-entering objects like common meteoroids, but still valid for our artificial meteoroids re-entering at 8 km/s.

D Release altitudes

An important aspect of the mission is to define the landing area of each possible artificial meteoroid. From the second stage, we have simulated with DRAMA the re-entry of the rocket stage and six different meteoroids without ablation. The SCARAB simulations show that the second stage will not undergo substantial mass loss: less than 80 kg on a total 1 ton. The artificial meteoroids have diameters of 5, 10, and 20 cm and densities of 7870 and 2400 kg/m^3. For the simulation we used as initial condition the state after the re-entry burn of the Spectrum rocket, given by Isar Aerospace, at an al-

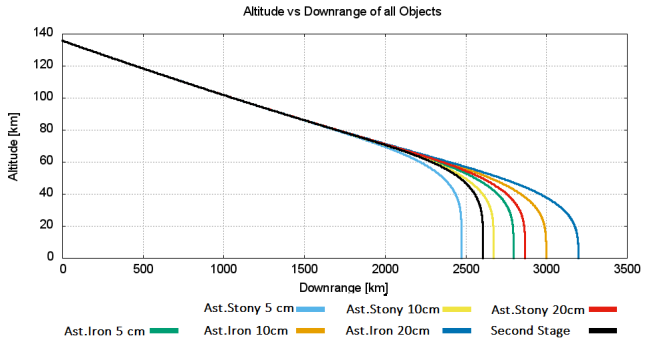

Figure 2 – SARA simulations of AllBert EinStein artificial meteoroids detaching at 500 km. The simulation results show that all artificial meteorites are within 600 km from the second stage landing zone.

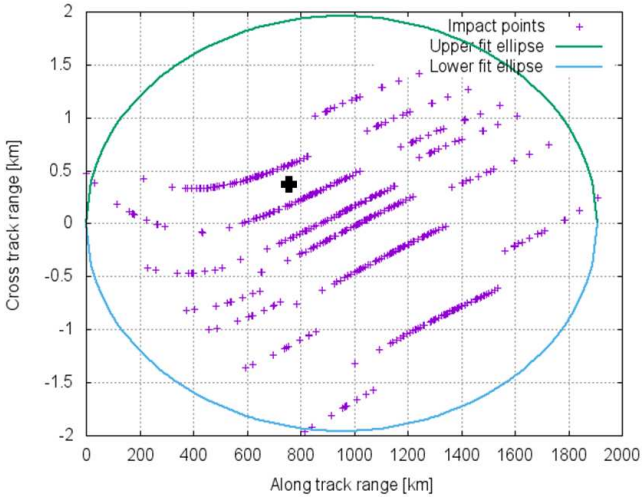

Figure 3 – SARA Monte Carlo simulations for a detaching altitude of 500 km. The black cross indicates the assumed landing position of the second stage. The purple crosses show the possible variation in the landing positions of the different artificial meteorites based on the randomized initial detaching velocities.

titude of 500 km from an SSO inclined at 97.°5, with an initial velocity of 7.54 km/s and an initial zenith angle of 89.°99. This is shown in Figure 2. Since we do not know exactly the re-entry position, all simulations were run from a starting latitude $\varphi = 0°$ and starting longitude $\lambda = 180°$.

The simulations, shown in Figure 2, demonstrate that all the artificial meteorites will be within 600 km from the rocket stage landing position. This is mainly because the acceleration toward Earth of each re-entry body will be the same until the air density will be sufficiently high to start drag deceleration. From that point onward, the ballistic coefficient $BC = m/(c_D S)$, where m is the mass of the body, c_D the drag coefficient, and S the cross-section area of the body, will play a major role in each object trajectory. Since the injection orbit may slightly vary, we have considered possible variations for the re-entry. Slight zenith angle variations do not influence the landing position and neither do slight changes of the orbital inclination. However, for small decreases in initial velocity, in the order of m/s, the landing position changes substantially.

Considering that the velocity will be the main driving factor in the variation of the re-entry position, and that we do not know which direction our payload will face in the fairing, we define the possible area where the artificial meteoroid will land based on the SARA Monte Carlo simulations. This is shown in Figure 3. We have chosen a value of 2 m/s as the standard deviation of the random Monte Carlo simulations, since we assume that the cage will detach with a separation velocity of about ±2 m/s.

From the simulation, we see that the constraint zone is reduced, especially after 200 km where the along-track and across-track distances do not vary a lot. This means that, after 200 km, the detaching velocity will not have significant influence on the meteoroid trajectory, and that the results will be just like the ones shown in Figure 2. For the rest of the computations, we have set the detaching altitude at 130 km mainly to reduce the computation time, but the same results will be valid for any other releasing altitude below 200 km.

E Airborne campaign

We have run a set of simulations based on the local observer point of view. In SCARAB, we have defined the mass loss in the re-entry of the second stage, the cage structure, and for each artificial meteoroid. Based on the mass loss data, we have defined the magnitude based on a maximum luminosity efficiency of $\tau = 0.1$ and a minimum luminosity efficiency of $\tau = 0.001$. Detaching from the upper stage at 130 km, the re-entry objects will have a velocity of 7.97 km/s and will fall with a zenith angle of 88.°17 and an inclination of the re-entry orbit of 97.°5.

As can be seen in Figure 4, the complete ablation of the aluminum cage structure needed to keep the object in place will occur well before the artificial meteoroid will start the ablation process. The artificial meteoroids ablate when their velocity is around 7.5 km/s. This is

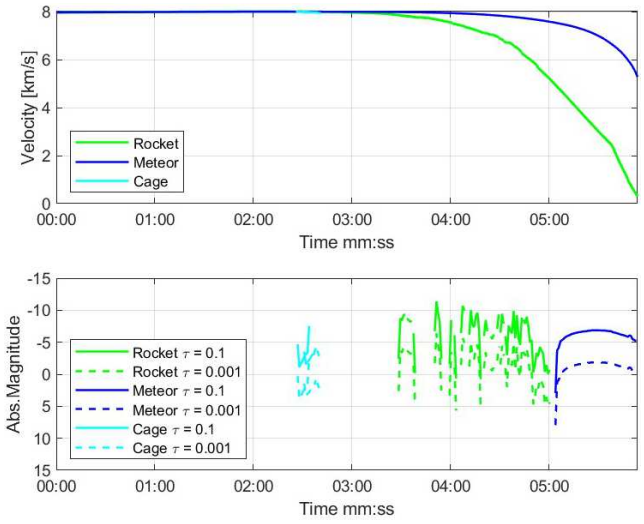

Figure 4 – Velocity and absolute magnitude over time of the rocket, cage, and meteor of a 10 cm iron artificial meteoroid, showing at what velocity the object will ablate.

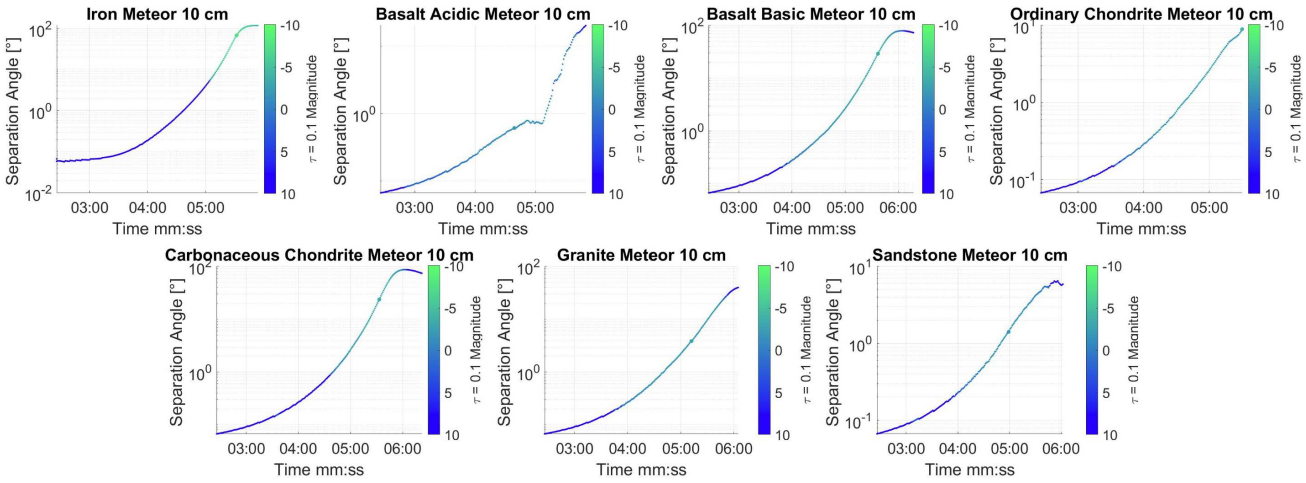

Figure 5 – Separation angle plot of 10 cm artificial meteoroid based on the possible material for the mission. The bigger dot shows the maximum brightness at the re-entry.

in general the velocity that a common slow meteor with an entering velocity of 11.2 km/s would have at the very end of the ablation.

The airborne observing campaign is set at an altitude of 10 km above the Earth's surface, to avoid cloud coverage. Using the observer's position, we can define the separation angle of the meteoroid and the second stage base with the cosine law. An angular distance of 0.°5, corresponding to the size of the Full Moon, has been considered as sufficient to distinguish the fireballs.

The different observing positions with respect to the re-entry position of the second stage entail different pros and cons. In front of the landing site of the second stage (with respect to the direction of re-entry), the observer will have a higher separation angle from the rocket at the start of the ablation, but the observed meteor will be rather weak, and the object will approach the horizon very rapidly. Behind the landing site of the second stage, the observed meteor will be brighter and most of the ablation will take place far away from the horizon, but the observer will have smaller separation angle from the rocket at the start of the ablation. Based on this trade-off, we have selected the observer position at 0.°3 in latitide to the south and 0.°3 in longitude to the east from the re-entry position of the second stage, because of the high brightness of the meteor, and because it passes far away from the horizon while having a sufficiently high separation angle from the rocket at the start of the meteoroid ablation.

Based on the position of the observer at 0.°3 in latitide to the south and 0.°3 in longitude to the east from the re-entry position of the second stage, we now focus on the brightness of the meteor. From the SCARAB results, we can exclude any 5 cm artificial meteors: they will be engulfed in the rocket fireball and will be quite hard to distinguish since they will ablate completely before their separation angle is bigger than 0.°5. So either a 10 cm or a 20 cm size ball would be a viable option. However, by considering that we need to limit as much as possible the volume and mass of the mission payload in order to facilitate the cage model, it should be better to avoid using 20 cm artificial meteoroids.

For 10 cm size spheres, all materials ablate far away from the rocket, and, for a multiple launch, the best results can be achieved with iron, basic basalt, carbonaceous chondrite, and sandstone (see Figure 5). The iron artificial meteoroid due to its high density would have a very high ballistic coefficient BC. The rest of the stony material, as show in Table 1, has densities that vary between 2000 and 3100 kg/m^3 but what really distinguishes them from each other is their high melting point. The carbonaceous chondrite has an especially high melting point $T_{\rm melt}$, while the basic basalt and sandstone have a very high specific heat of melting $H_{\rm melt}$, making it hard to lose mass in the ablation.[a]

Based on these selected artificial meteoroids, the mission layout can be plotted as shown in Figure 6. The iron and the sandstone are well distinguishable from the others while the carbonaceous chondrite and basic basalt have a similar density of respectively 2800 and

[a]The raw SCARAB simulations data selected are freely available at `https://data.mendeley.com/datasets/mdtwk5bxn5/1`.

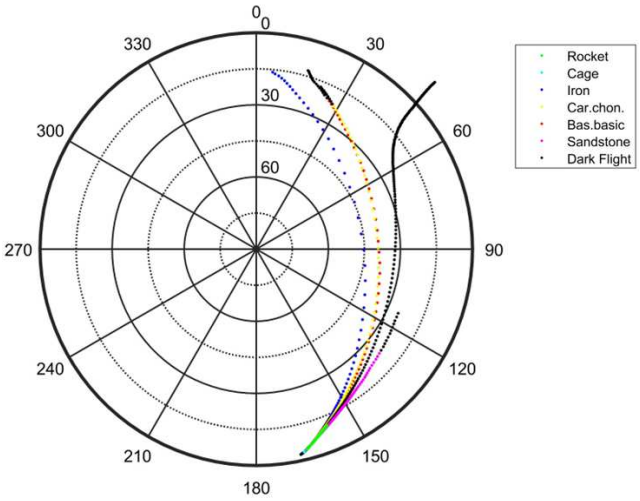

Figure 6 – Azimuth/elevation plot showing possible trajectories of the fireball observed by the airborne campaign for 10 cm artificial meteoroids, depending on the material used for the mission. The black dots represent the dark flight of the objects.

3100 kg/m^3, giving them a very similar ballistic coefficient BC. In order to increase the angular distance between both, we would have to increase the difference in BC by varying their size or mass.

F Conclusions

The study shows the feasibility of the AllBert EinStein mission based on the material properties and ballistic coefficients of the artificial meteoroids using the software of the ESA's space debris community for artificial meteoroid simulations.

For detaching altitude lower than 200 km, the reentry positions will no longer be influenced by the detaching velocity, but will only depend on the artificial meteoroid's ballistic coefficient BC. Furthermore, the difference between the ballistic coefficient BC of the meteoroid and the rocket stage will help distinguish the two fireballs. From the simulations, we can infer that the artificial meteoroid's diameter must be more than 5 cm to avoid that the artificial meteoroid will ablate too close to the second stage. Moreover, the best suited materials for the mission should have very different densities in order to have different ballistic coefficients BC. Also, the artificial meteoroid materials should have a high melting temperature T_{melt}, between 1700 and 2000 K, or a very high specific heat of melting H_{melt}, over 500 000 J/kg, with in general a very high specific heat capacity c_p of about 1000 J/(kg.K) to reach their melting temperature faster.

Acknowledgements

The authors would like to acknowledge the support of, and give their warmest thanks to, the whole team of Hyperschall Technologie Göttingen GmbH (HTG), which allowed us to use the SCARAB software.

They also thank Isar Aerospace for the data given on the re-entry simulations of their Spectrum rocket.

Finally, thanks go to Vitali Braun for his advice about space debris and Stefan Loehle for suggestions on possible types of materials.

References

Abdulagaov I. M., Abdulagatova Z. Z., Kallaev S. N., and Omarov Z. M. (2019). "Heat-capacity measurements of sandstone at high temperatures". *Geomechanics and Geophysics for Geo-Energy and Geo-Resources*, **5:1**, 65–85.

Bouhifd M. A., Besson P., Courtial P., Gerardin C., Navrotsky A., and Richet P. (2007). "Thermochemistry and melting properties of basalt". *Contributions to Mineralogy and Petrology*, **153:6**, 689–698.

Ceplecha Z., Borovička J., Elford W. G., ReVelle D. O., Hawkes R. L., Porubčan V., and Šimek M. (1998). "Meteor phenomena and bodies". *Space Science Reviews*, **84:3**, 327–471.

Frühauf M., Gscheidle C., and Koschny D. (2022). "AllBert EinStein". `https://www.asg.ed.tum.de/en/lpe/research/near-earth-objects-and-impacts/allbert-einstein/` . Viewed 27 February 2023.

Gilmour C. M., Freemantle J., and Daly M. G. (2020). "Thermal conductivity of asteroid analogue material". In *51st Lunar and Planetary Science Conference*, number 2326. page 2354.

Hartlieb P., Toifl M., Kuchar F., Meisels R., and Antretter T. (2016). "Thermo-physical properties of selected hard rocks and their relation to microwave-assisted comminution". *Minerals Engineering*, **91**, 34–41.

Kanzler R., Lips T., Fritsche B., Pontijas Fuentes I., Bonetti D., Letterio F., De Miguel G. V., Blanco Arnao G., Palomo P., Parigini C., et al. (2017). "Upgrade of drama's spacecraft entry survival analysis codes". In Flohrer T. and Schmitz F., editors, *7th European Conference on Space Debris (ECSD)*. Darmstadt, Germany, 18–21 April 2017. ESA Space Debris Office.

Lesher C. E. and Spera F. J. (2015). "Thermodynamic and transport properties of silicate melts and magma". In Sigurdsson H., Houghton B., McNutt S., Rymer H., and Stix J., editors, *The encyclopedia of volcanoes*, pages 113–141. Elsevier.

Lips T., Fritsche B., Breslau A., and Kärräng P. (2019). "Final report : Upgrade of DRAMA's spacecraft entry survival analysis codes". *Hyperschall Technologie Göttingen*.

Lips T., Fritsche B., Homeister M., Koppenwallner G., Klinkrad H., and Toussaint M. (2007). "Re-entry risk assessment for launchers–development of the new SCARAB 3.1 L". In Danesy D., editor, *Proceedings of the 2nd IAASS Conference, SP-645, ESA Communication Production Office, ESTEC, Noordwijk, The Netherlands*.

Loehle S., Zander F., Hermann T., Eberhart M., Meindl A., Oefele R., Vaubaillon J., Colas F., Vernazza P., Drouard A., et al. (2017). "Experimental simulation of meteorite ablation during Earth entry using a plasma wind tunnel". *The Astrophysical Journal*, **837:2**, 112.

Opeil C. P., Britt D. T., Macke R. J., and Consolmagno G. J. (2020). "The surprising thermal properties of cm carbonaceous chondrites". *Meteoritics & Planetary Science*, **55:8**, E1–E20.

Szurgot M. (2011). "On the specific heat capacity and thermal capacity of meteorites". In *42nd Annual Lunar and Planetary Science Conference*, number 1608. page 1150.

Szurgot M. (2012). "On the heat capacity of asteroids, satellites and terrestrial planets". In *43rd Lunar and Planetary Science Conference*, number 1659. page 2626.

Handling Editor: Marc Gyssens

This paper has been typeset from a LaTeX file prepared by the authors.

The Flying Fish Fireball of 2014 July 17

Mark E. Bailey[1], *Apostolos A. Christou*[2] *and James A. Finnegan*[3]

Observations of the bright (absolute magnitude approximately −5.6) fireball of 2014 July 17, $01^h59^m26^s$ (UT), seen from England, Scotland and Northern Ireland are presented. Among various visual reports the fireball was recorded by the NEMETODE (Network for Meteor Triangulation and Orbit Determination) system (`http://www.nemetode.org`) and other cameras. The meteor was unusual in showing a white spray beyond the main meteor head, bright colours, and a shape resembling a flatfish such as a manta or sting ray. The intense green or cyan colour of the fireball suggests ablation from a meteoroid with an underlying stony-iron or nickel-iron composition.

Received 2023 March 16

A Introduction

The interesting paper by Slansky (2022) describing the morphology of meteor halos reminded us of the remarkable 'flying fish' fireball that was seen from England, Scotland and Northern Ireland at around 02:00 (UT) on 2014 July 17. At this time, the Armagh Observatory's meteor cameras had been operating for approximately nine years and its all-sky cameras had been operating continuously for about a year (`http://allsky.zapto.org/`). One of the Observatory's instruments recorded the fireball, as too did cameras operating as part of the NEMETODE system (Stewart et al., 2013), of which one at least had been operating from as early as 2010.

Visual descriptions of this and similarly bright meteors can be found, for example, in Armagh Observatory's database of fireball reports and in the meteor section reports of the Society for Popular Astronomy (`https://www.popastro.com/`) and the British Astronomical Association (`https://britastro.org`), not to mention in newspapers, radio and television, and on social media. The Observatory's fireball report form and anonymised reports can be viewed on archived copies of its previous website (e.g., `https://t.ly/VbMT`). We found that fireball reports were a valuable tool for engaging members of the public in astronomy and space science. A completed report together with the observer's name and contact details enabled astronomers to obtain further information about specific events when necessary and to give feedback explaining what had been seen. The fireball reports became an information resource supplementing traditional (and less frequent) public queries received by post or telephone.

As well as meteors, we found that people sometimes reported observations that could easily be explained in terms of distant aircraft or brightly shining contrails, bright planets such as Venus, fireworks or Chinese lanterns (especially around public holidays), and glints or 'Iridium flares' associated with artificial satellites. A cluster of reports describing the same event was a trigger to inspect output from the Observatory's meteor cameras and such reports were often found to describe a bright meteor or fireball.

B Observations

One such report-cluster was associated with what we dubbed the 'flying fish' fireball. This was seen on 2014 July 17, $01^h59^m26^s$ (UT) and lasted some 6 or 7 seconds. A visual report from Salford, near Manchester, described a green fireball accompanied by a mixture of red and yellow with no sound, and with whitish streams like a vapour stream on the outside. Another observation, received around lunchtime on July 17th from Mansfield, Nottinghamshire, described the meteor as having an orange light with a blue tail travelling from west to east and lasting about 3 seconds till it went out with a cracking sound like a firework. A third report also received soon after the event described an object seen from Newtownards, Co. Down. This was said to be as bright as the full moon, mainly white but with a green centre and with parts breaking up during the time it was observed, probably around 2 seconds.

We immediately examined our all-Sky camera records for the night in question. Although one camera missed the event because it occurred during one of its inter-frame periods, the other, then being operated by a colleague (George Patton) near Emyvale, Co. Monaghan, obtained an image through cloud. Accordingly, we passed the observation to William Stewart who was coordinating reports on behalf of the NEMETODE project (`http://www.nemetode.org/`). He responded by drawing our attention to other observations, notably a video record by David Anderson from near Girvan, South Ayrshire, and his own video from Ravensmoor, near Nantwich, Cheshire (see `https://t.ly/_Uj-`). Further analysis suggested that the fireball was a sporadic with an absolute magnitude approximately −5.6 probably coming from a typical Apollo Earth-crossing orbit.

A few days later we received perhaps the most intriguing observation of the event. This began as a telephone query regarding a strange object seen in the sky while driving near Ballynahinch, Co. Down. The object was described as a 'flying fish', and in the observer's subsequent report for the fireball database (received on 2014 October 22) it was said to be shaped like a flatfish, fluorescent green and with a long red tail about a third

[1]Armagh Observatory and Planetarium.
Email: `mebailey_uk@btinternet.com`
[2]Armagh Observatory and Planetarium.
Email: `apostolos.christou@armagh.ac.uk`
[3]QSK Electronics, Richhill. Email: `finnegane32@aol.com`

IMO bibcode WGN-512-bailey-flyingfish
NASA-ADS bibcode 2023JIMO...51...38B

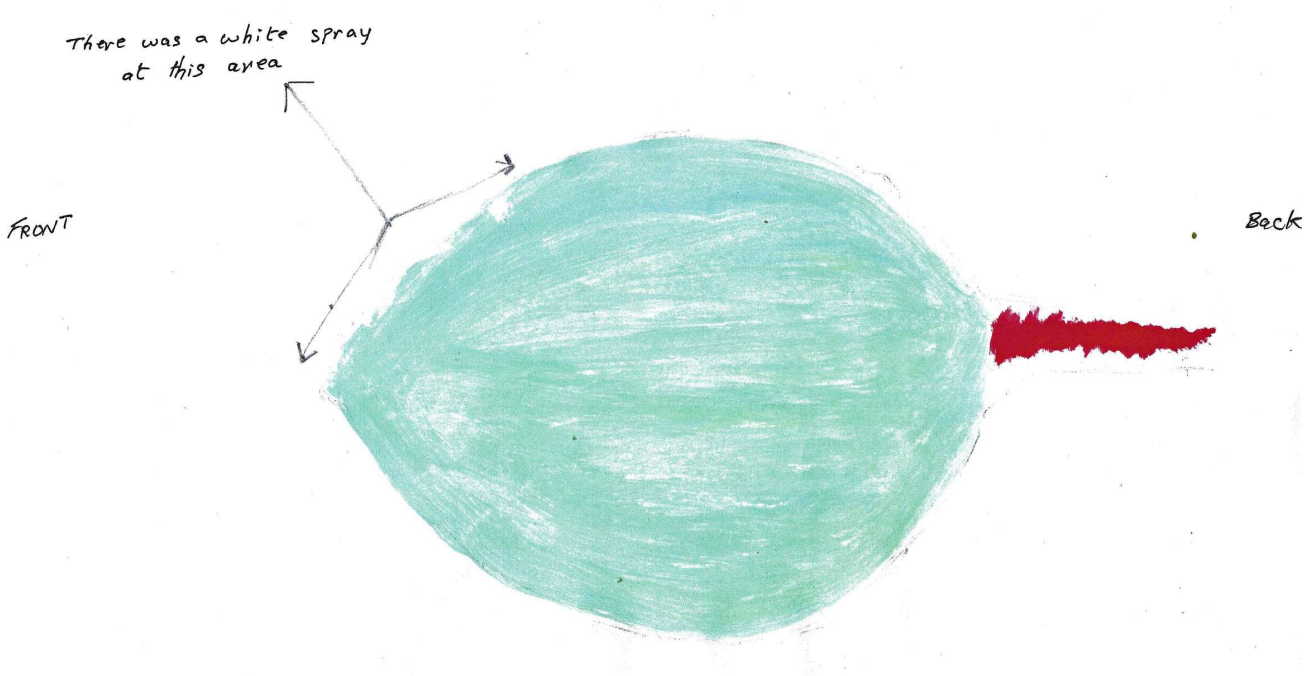

Figure 1 – The 'flying fish' fireball of 2014 July 17, $01^{h}59^{m}26^{s}$. The 'white spray' close to the leading edge of the meteor head was also mentioned in the independent visual report from Salford. It is possible that a careful analysis of William Stewart's original video might help to elucidate this structure. Drawing courtesy of Dennis Lennon.

the size of the main green shape. It travelled very fast and was observed for about 5 seconds.

In light of the previously received reports it was evident that this was the same fireball, although at the time the observer (Dennis Lennon) was adamant that it was not an ordinary meteor. Subsequently, he kindly produced a drawing of what had been seen, bringing it to the Observatory for review on July 31st. A copy of the drawing is shown in Figure 1. This provides independent visual confirmation of the unusual white spray or whitish streams seen beyond the main meteor. The observer's response on seeing William Stewart's video record of the fireball was words to the effect, "that was it!". This suggests that the video provided a recognisable and reasonably accurate portrayal of the visual appearance of the fireball.

Excerpts from William Stewart's video (see `https://t.ly/_Uj-`) showing the evolution of the apparent meteor head, halo, and tail are shown in Figure 2. The sequence begins by showing the development of a fairly unremarkable meteor with a bright teardrop or tadpole-like shape crossing just below the centre of the video field of view, but it goes on to display a more unusual 'delta' shape as the fireball moves from field centre towards the upper right corner of the video field. The early frames agree well with Dennis Lennon's drawing, but the last three show a more peculiar structure.

We thank Alex Pratt, William Stewart, and Peter Slansky for sharing their expertise and for taking time to review this unusual video sequence. They rightly urge caution against over interpreting such video records. Rather than showing the development of the underlying shape of the meteor head and halo, the changing shape of the meteor as it tracks across the video field of view can be attributed entirely to a combination of image distortions in the video camera system. Similarly, the apparent meteor halo shown in these images is most likely an artefact of 'blooming' caused by saturation of the image of the bright meteor rather than anything real.

This image sequence illustrates the potential of even ten-year old video technology to capture important details of the interaction of a bright fireball with the Earth's atmosphere. However, in this case, the evolution of the images, in particular the unusual 'delta' shape and 'butterfly' wings of the meteor head, are dominated by camera artefacts and lens distortions rather than anything real. This reinforces the need for higher quality video imaging of fireballs before the analysis of such images can be used as a ground for improving theories of the time-variable interaction of meteoroids with planetary atmospheres.

C Discussion

We bring these observations to a wider audience for several reasons. First, with improvement in the quality of meteor camera systems there is the prospect of obtaining copious high-quality video images showing the evolution of bright meteors. Such data could provide the basis for statistical studies of the time-variable development of bright fireballs and, where present, the extended meteor halo. The fireball's colour and flashes associated with the loss and/or disruption of fragments of the meteoroid (as indicated in the last frame of Figure 2) in turn provide information on the composition and cohesive strength of the meteoroid and its melting point, complementing orbital information routinely supplied by members of video camera networks.

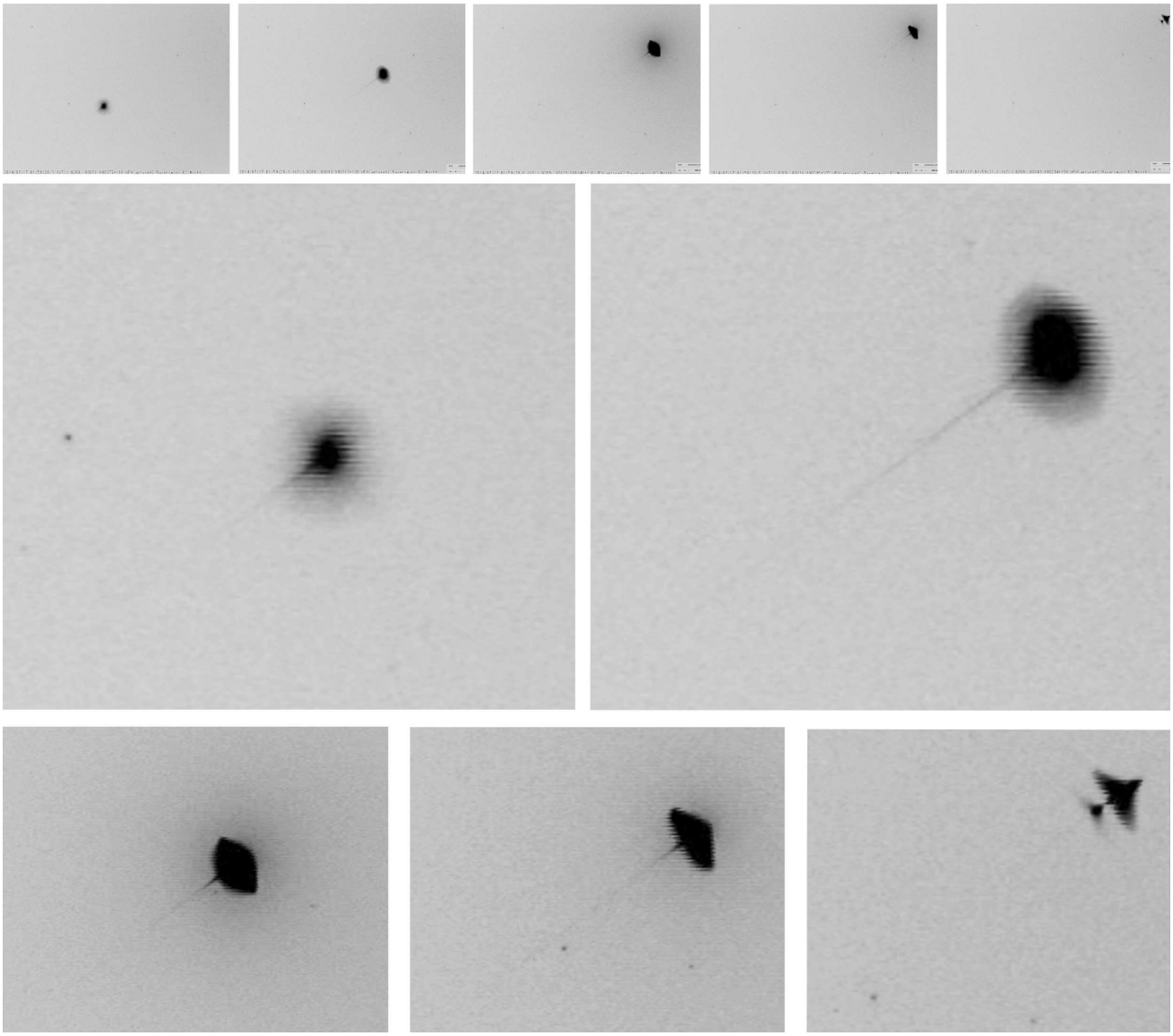

Figure 2 – Top: A sequence of 'stills' from William Stewart's video on the NEMETODE website showing the development of video images of the 'flying fish' fireball of 2014 July 17 over approximately 6 seconds from the start of the event around $01^{h}59^{m}26^{s}$. The top row shows the location of the images in the context of the video camera's field of view. Enlarged and cropped versions of these images are shown in the middle and bottom rows. The fireball entered near the lower left corner of the field of view crossing just below the field centre and and leaving near the upper right. The images are time-stamped at $01^{h}59^{m}\ldots$ $28^{s}.3$, $29^{s}.1$, $30^{s}.0$, $30^{s}.6$ and $31^{s}.1$ respectively. A bright fragmentation event occurred at approximately $31^{s}.0$ leading to two main components of the meteor as shown in the last frame (cropped version bottom right). Centre and Bottom: Enlarged and cropped examples of the same frames. As with the exact shape of the fireball in the video images, we emphasize that the apparent meteor halo is most likely instrumental, an artefact of blooming and lens distortions in this video camera.

Secondly, the whitish streams or spray seen beyond the main body of the meteor were independently confirmed by two visual observers, suggesting a real phenomenon. The cause of this emission, which appears not yet to have been unambiguously detected by current meteor camera systems, remains uncertain as too does the frequency of its occurrence among bright fireballs. This highlights the importance of visual observations of bright fireballs and the need to assess and archive the best visual reports.

Thirdly, one of the observers reported a 'cracking' sound, which suggests that this unusual fireball may have been an example of an electrophonic meteor (e.g., Finnegan 2015).

Lastly, although the intense green colour of the flying fish fireball is not unique it is recognised (e.g., Bone 1993) as reasonably rare. Other 'green' fireballs recently observed from or over the UK include those of 2017 December 31, $17^{h}33^{m}$, 2022 May 11, $23^{h}40^{m}$, and 2022 September 14, $22^{h}00^{m}$. At least one of these (that of 2017 December 31) also showed a red tail (e.g., `https://t.ly/NJTm`).

In the absence of a detailed spectrum, we wonder what generally can be deduced from this and other visual observations of meteor colours, and in this case also the red tail. Visual reports of the colours of bright meteors, as in the case of shower meteors, might help to suggest possible connections between the different kinds

of fireball and their orbits. In the case of the flying fish we suggest that the green head was probably caused by magnesium or nickel, suggesting ablation of a rare stony-iron or nickel-iron meteoroid, while the red tail was most likely produced by atmospheric molecular nitrogen or perhaps atomic oxygen, a minor constituent of the Earth's atmosphere at meteor heights.

Acknowledgements

We thank members of the public for reporting varied observations to the fireball database, and especially Dennis Lennon for drawing what he saw. We also thank Javor Kac for encouraging us to consider the effects of image distortion near the edge of a meteor camera system's field of view, and William Stewart, Alex Pratt, and Peter Slansky for sharing their knowledge and expertise. This has significantly improved the paper. In particular, it was William Stewart's video and the NEMETODE system which, nine years ago, enabled us promptly to confirm that the 'flying fish' was a fireball.

References

Bone N. (1993). *Philip's Observer's Handbook: Meteors.* George Philip Ltd, London, 176 pages. (see p.73).

Finnegan J. A. (2015). ""Hiss, clicks and pops" – The enigmatic sounds of meteors". *WGN, Journal of the IMO*, **43:2**, 47–57.

Slansky P. C. (2022). "Meteor halo phenomena — attempt at a morphological classification". *WGN, Journal of the IMO*, **50:6**, 165–178.

Stewart W., Pratt A. R., and Entwisle L. (2013). "NEMETODE: The Network for Meteor Triangulation and Orbit Determination. System overview and initial results from a UK video meteor network". *WGN, Journal of the IMO*, **41:3**, 84–91.

Handling Editor: Javor Kac
This paper has been typeset from a LaTeX file prepared by the authors.

An analysis of the records of remarkable meteors along 2022 from the PatrICIA project

Rodolfo Langhi[1,2], *Helena Ferreira Carrara*[1,3] *and Tainá Bueno de Andrade*[1,4]

In this paper, we present the preliminary results of the meteor monitoring station of the Astronomical Observatory of São Paulo State University (Unesp), in partnership with the Brazilian Meteor Observation Network (BRAMON), from 2022 January 26 to the same date in 2023. We recorded a total of 78 meteors and an average of 1.4 meteors per night. The faintest meteor magnitude was 2.5 and the brightest meteor magnitude was −6.0, and the month of May had the highest number of records.

Received 2023 March 27

A Introduction

The Astronomical Observatory from São Paulo State University (Unesp), School of Sciences, Bauru city (Brazil) has a systematic monitoring station of meteors since january of 2022, whose research is being carried out within the scope of the project PatrICIA (in Brazilian Portuguese: Patrulhamento Investigativo do Céu por Imageamento Automático; in English: Investigative Auto Imaging Sky Patrol). Our station is part of a brazilian network of stations called BRAMON (Brazilian Meteor Observation Network) created in 2014 and, nowadays, with 93 stations around the country.

This paper focuses on preliminary analysis of the records of the brightest meteors captured by our station within a year period. Other results and different conclusions of this project may be found in Andrade (2021), Carrara (2021), Carrara and Langhi (2022).

The start of its operation was on 2022 January 7, but the data contained in this article cover the period of exactly one year, and it is appropriate, by the data obtained, from 2022 January 26 to the same date of 2023.

The analyses of these observations allow us to derive important information of showers and sporadic meteors and thus contribute to meteor data in the southern hemisphere, where there is a reduced amount of research (Jenniskens et al., 2018).

B Equipment and methods

The records reported in this paper were obtained by our station, which uses a SCB-2000 Samsung camera associated with a lens $f/D = 1$ with auto iris, directed to the northeast horizon, centered on azimuth 51° and elevation 29°, covering a field of view of 80° × 55°. The system is connected to a common desktop computer with the softwares UFOCapture and UFOAnalyser (SonotaCo).

All equipment is installed in the building of the Unesp Didactic Astronomy Observatory, at the coordinates 22.3582971° South and 49.0272581° West, at an altitude of 632.57 meters, located in the city of Bauru, State of São Paulo, Brazil, in the time zone GMT−3h, as described in the observatory homepage: `https://www.fc.unesp.br/observatorio`.

Figure 1 – Meteor monitoring station of the PatrICIA project of the Astronomy Observatory of São Paulo State University (Unesp), School of Sciences, Bauru (Brazil).

C Analysis of the records

As previously mentioned, the results presented here refer to the period of one year and, in this interval, a total of 78 meteors were detected. It is important to note that not every night provides data due to factors such as periods of shower, cloudy skies and problems with the camera. There were 56 nights we got at least 1 record, so an average of 1.4 meteors per night.

According to the above in Figure 2, in May we reached the highest number of meteors recorded, while in September and December the minimum number of meteors were recorded.

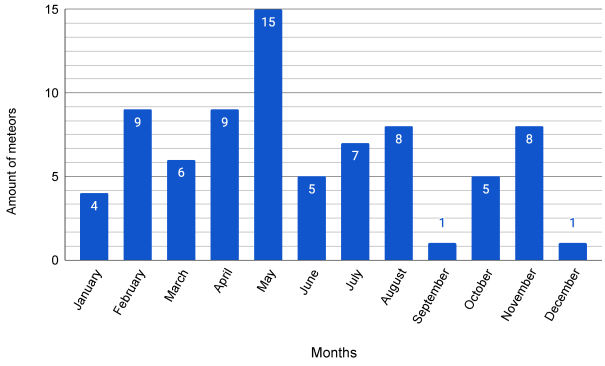

Figure 2 – Quantity of meteors within the months.

[1]Astronomical Observatory of São Paulo State University (Unesp), School of Sciences, Physics Dept., 17033-360, Brazil.
[2]Email: `rodolfo.langhi@unesp.br`
[3]Email: `hf.carrara@unesp.br`
[4]Email: `bueno.andrade@unesp.br`

IMO bibcode WGN-512-langhi-patricia
NASA-ADS bibcode 2023JIMO...51...42L

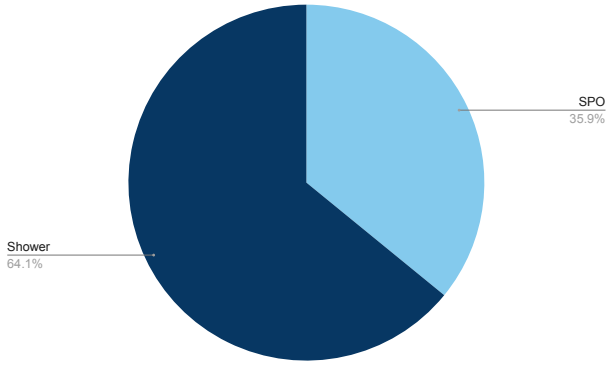

Figure 3 – Percentage of meteors regarding showers or sporadic.

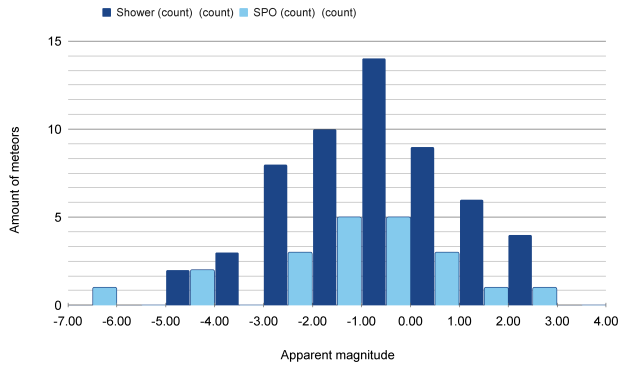

Figure 4 – Quantity of meteors x Apparent Magnitude.

Figure 3 shows that most meteors (64.1%) came from showers already known and cataloged by the IAU, and the minority of these meteors detected (35.9%) were sporadic (SPO).

It is also interesting to note that the showers with the highest meteor detections were ATH (April 21 Herculids) and MKQ (May kappa Aquariids), with 3 meteors in each. Another 5 showers had 2 meteors detected each, and the rest of the meteor showers were prepresented by only 1 meteor.

Attention is needed for the acronyms of the radiant showers, because, as shown, it's the data of only one station, so it's a statistical estimate from single station tracks. To have accurate data, these data have to be computed from triangulation with other stations facing the same direction.

As for the apparent magnitudes of the meteors, it is verified that the overall average magnitude was −0.89, the faintest magnitude recorded was +2.5, while the brightest meteor was a bolide of magnitude −6.0.

It is also verified that the faintest and brightest magnitudes were rarely reached, with the majority of meteors between the magnitudes of −2.0 and +1.0.

The annual average magnitude of meteors, specifically those from showers is −0.74 and the annual average of sporadic sands is −1.29. Therefore, the brightest meteors captured by the station were the sporadic ones.

Looking at Figure 7, it is noted that the amount of meteors was higher after $03^{h}00^{m}$ UT (midnight local time), 18 meteors were recorded before $03^{h}00^{m}$ a.m. and 60 after this time.

Figure 5 – Meteor with the brightest magnitude detected (−6.0).

Figure 6 – Meteor with the faintest magnitude detected (+2.5).

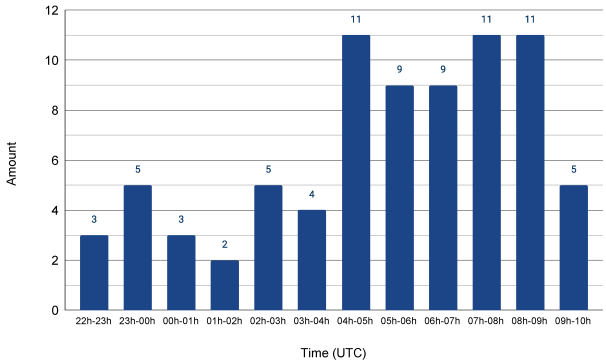

Figure 7 – Quantity of meteors by time range.

Figure 8 – Meteor with magnitude −2.47 on 2022 July 11.

Finally, we brought Figure 8 to exemplify one of the representative images of the project. Compared to the meteor in Figure 5, it looks like this one is brighter. However, the photo is the result of the camera's position relative to the direction of the meteor. The measurements and records obtained through the analysis carried out by the software show that the meteor of 2022 July 11 (Figure 8), in fact, was not brighter than the meteor of 2022 November 9 (Figure 5).

D Conclusions

Our station recorded a total of 78 meteors over the course of a year. Really, it's not a surprising amount, considering the nights when the equipment was under maintenance or the coverage of 100% cloudiness, besides the fact that our station has only a single camera with a visual field of $80° \times 55°$. We started to work in 2022 January, so that the station is recent and awaits future expansions and improvements. However, even so, it has already been possible to obtain the preliminary results presented in this paper.

References

Andrade T. B. (2021). "Estudo de meteoros com o projeto patricia". *Interfaces da educação em astronomia*, **2**, 239–254.

Carrara H. F. (2021). "Projeto caça asteroides: resultados que superam a descoberta de asteroides". *Interfaces da educação em astronomia*, **2**, 255–271.

Carrara H. F. and Langhi R. (2022). "Educação em astronomia para a formação do cidadão cientista". *CIC Unesp*, **34**, 107.

Jenniskens P., Baggaley J., Crumpton I., Aldous P., Pokorny P., Janches D., Gural P. S., Samuels D., Albers J., Howell A., Johannink C., Breukers M., Odeh M., Moskovitz N., Collison J., and Ganju S. (2018). "A survey of southern hemisphere meteor showers". *Planetary and Space Science*, **154**, 21–29.

Handling Editor: Javor Kac

The International Meteor Organization

www.imo.net

Follow us on Facebook InternationalMeteorOrganization

Follow us on Twitter @IMOMeteors

Council

President: Cis Verbeeck,
Bogaertsheide 5, 2560 Kessel, Belgium.
e-mail: cis.verbeeck@gmail.com

Vice-President: Juraj Tóth,
Fac. Math., Phys. & Inf., Comenius Univ.,
Mlynska dolina, 84248 Bratislava, Slovakia.
e-mail: toth@fmph.uniba.sk

Secretary-General: Robert Lunsford,
14884 Quail Valley Way, El Cajon,
CA 92021-2227, USA. tel. +1 619 755 7791
e-mail: lunro.imo.usa@cox.net

Treasurer: Marc Gyssens, Heerbaan 74,
B-2530 Boechout, Belgium.
e-mail: marc.gyssens@uhasselt.be
BIC: GEBABEBB
IBAN: BE30 0014 7327 5911
Bank transfer costs are always at your expense.

Other Council members:
Karl Antier, 16, rue de la République,
F-04100 Manosque, France.
e-mail: karl.antier@gmx.fr
Javor Kac (see details under WGN)
Detlef Koschny, Zeestraat 46,
NL-2211 XH Noordwijkerhout, Netherlands.
e-mail: detlef.koschny@tum.de
Sirko Molau, Abenstalstraße 13b, D-84072
Seysdorf, Germany. e-mail: sirko@molau.de
Francisco Ocaña Gonzalez, C/ Arquitectura, 7.
28005 Madrid, Spain.
e-mail: francisco.ocana.gonzalez@gmail.com
Vincent Perlerin, 16, rue Georges Bernanos,
51100 Reims, France.
e-mail: vperlerin@gmail.com
Jürgen Rendtel, Eschenweg 16, D-14476
Marquardt, Germany. e-mail: jrendtel@aip.de

Commission Directors

Visual Commission: Jürgen Rendtel
Generic e-mail address: visual@imo.net
Electronic visual report form:
http://www.imo.net/visual/report/electronic
Video Commission: Sirko Molau (video@imo.net)
Photographic Commission: Bill Ward
(bill_meteor@yahoo.com)
Generic e-mail address: photo@imo.net
Radio Commission: Chris Steyaert
(radio@imo.net)
Fireball Commission: Robert Lunsford
Online fireball reports:
http://fireballs.imo.net

Webmaster

Karl Antier, e-mail: webmaster@imo.net

WGN

Editor-in-chief: Javor Kac
Na Ajdov hrib 24, SI-2310 Slovenska Bistrica,
Slovenia. e-mail: wgn@imo.net;
include METEOR in the e-mail subject line

Editorial board: Ž. Andreić, D.J. Asher,
F. Bettonvil, M. Gyssens, C. Hergenrother,
T. Heywood, J. Rendtel, C. Verbeeck,
S. de Vet, D. Vida.

IMO Sales

Available from the Treasurer or the Electronic Shop on the IMO Website	€	$
IMO membership, including subscription to WGN Vol. 51 (2023)		
Surface mail	26	30
Air Mail (outside Europe only)	49	56
Electronic subscription only	21	24
Proceedings of the International Meteor Conference on paper		
1990, 1991, 1995, 1996, 1999, 2000, 2002, 2003, per year	9	12
2007, 2010, 2011, per year	15	20
2012, 2013, 2015, 2017 per year	25	32
Proceedings of the Meteor Orbit Determination Workshop 2006	15	20
Radio Meteor School Proceedings 2005	15	20
Handbook for Meteor Observers	23	29
Meteor Shower Workbook	12	16
Electronic media		
Meteor Beliefs Project ZIP archive	6	8

Meteorite-dropping fireball of 2023 February 13